

Reaction Coupling through Interdomain Contacts in Imidazole Glycerol Phosphate Synthase[†]

Rebecca S. Myers,^{‡,⊥} Rommie E. Amaro,^{§,⊥} Zaida A. Luthey-Schulten,^{§,||} and V. Jo Davisson^{*,‡}

Department of Medicinal Chemistry & Molecular Pharmacology, Purdue University, West Lafayette, Indiana 47907-2091, and Department of Chemistry, Beckman Institute, University of Illinois at Urbana-Champaign, Urbana, Illinois 61801

Received April 18, 2005; Revised Manuscript Received June 23, 2005

ABSTRACT: Imidazole glycerol phosphate (IGP) synthase, a triad glutamine amidotransferase, catalyzes the fifth step in the histidine biosynthetic pathway, where ammonia from glutamine is incorporated into *N*¹-[(5′-phosphoribulosyl)-formimino]-5-aminoimidazole-4-carboxamide ribonucleotide (PRFAR) to yield IGP and 5′-(5-aminoimidazole-4-carboxamide) ribonucleotide (AICAR). The triad family of glutamine amidotransferases is formed by the coupling of two disparate subdomains, an acceptor domain and a glutamine hydrolysis domain. Each of the enzymes in this family share a common glutaminase domain for which the glutaminase activity is tightly regulated by an acceptor substrate domain. In IGP synthase the glutaminase and PRFAR binding sites are separated by 30 Å. Using kinetic analyses of site-specific mutants and molecular dynamic simulations, we have determined that an interdomain salt bridge in IGP synthase between D359 and K196 (approximately 16 Å from the PRFAR binding site) plays a key role in mediating communication between the two active sites. This interdomain contact modulates the glutaminase loop containing the histidine and glutamic acid of the catalytic triad to control glutamine hydrolysis. We propose this to be a general principle of catalytic coupling that may be applied to the entire triad glutamine amidotransferase family.

Imidazole glycerol phosphate (IGP)¹ synthase catalyzes the fifth step in the histidine biosynthetic pathway, where the unusual nucleotide, *N*¹-[(5′-phosphoribulosyl)-formimino]-5-aminoimidazole-4-carboxamide ribonucleotide (PRFAR), is transformed to IGP and 5′-(5-aminoimidazole-4-carboxamide) ribonucleotide (AICAR). A condensation reaction with ammonia derived from the hydrolysis of glutamine promotes the requisite carbon–nitrogen ligation and cyclization to form the imidazole ring of the final metabolic product, histidine (Figure 1) (1). The structure of IGP synthase utilizes the (β/α)₈ barrel motif to bind PRFAR and functions as a cyclase domain. Glutamine is bound some 30 Å away in a triad amidotransferase domain (3–5). The structural relationship of the (β/α)₈ barrel to the amidotransferase domain in IGP synthase is especially important for function since it

has been strongly implicated as a channel for transferring ammonia between active sites (6, 7). The interdomain region in the structure of IGP synthase from *S. cerevisiae* buries approximately 1700 Å² of surface area from the two domains and defines an ammonia chamber (3, 8). In addition, several interdomain contacts are revealed in this structure and offer a mechanistic basis for study of the underlying dynamic features of the protein that enable coordinated regulation of the catalytic properties in each active site.

As a member of the family of triad glutamine amidotransferases, IGP synthase shares a common protein fold that contains the active site for glutamine hydrolysis (2, 9). A conserved triad of amino acids composed of a cysteine at approximately position 85 residing in a conserved CXGXQ motif, and a histidine and glutamic acid approximately 90 residues downstream catalyzes glutamine hydrolysis. The utilization of a common protein fold in the glutaminase domain has led to the theory that the glutamine amidotransferases have evolved through gene duplication. Ancestral proteins in each subfamily of acceptor domains were likely ammonia-dependent proteins that utilized exogenous ammonia in their synthesis reactions. The functional association of a glutamine hydrolyzing protein then assured a steady source of ammonia, resulting in a greater abundance of essential building blocks for growth and replication (2). In review of the six triad glutamine amidotransferase structures solved to date (3, 10–14), it is apparent that a common face of the amidotransferase domain docks onto the divergent acceptor domains. The fused IGP synthase from yeast offers a particular advantage for understanding the structure–function relationships of the amidotransferase interface as a

[†] This work was supported by National Institutes of Health grant RO1 GM067915 to V.J.D., National Science Foundation Grant MCB02-35144 and National Resource Allocation Committee Grant MCA03-50275 to Z.L.-S.

* Correspondence to Department of Medicinal Chemistry & Molecular Pharmacology, Purdue University, 575 Stadium Mall Dr., West Lafayette, IN 47907-2091, 765-494-5238 (Office), 765-494-1414 (Fax), davisson@purdue.edu.

[‡] Purdue University.

[§] Department of Chemistry, University of Illinois at Urbana-Champaign.

^{||} Theoretical and Computational Biophysics Group, University of Illinois at Urbana-Champaign.

[⊥] These authors contributed equally to this work.

¹ Abbreviations: AICAR, 5′-(5-aminoimidazole-4-carboxamide) ribonucleotide; EDTA, ethylenediaminetetraacetic acid; IGP, imidazole glycerol phosphate; PIPES, 1,4-piperazinediethanesulfonic acid; PRFAR, *N*¹-[(5′-phosphoribulosyl)-formimino]-5-aminoimidazole-4-carboxamide ribonucleotide.

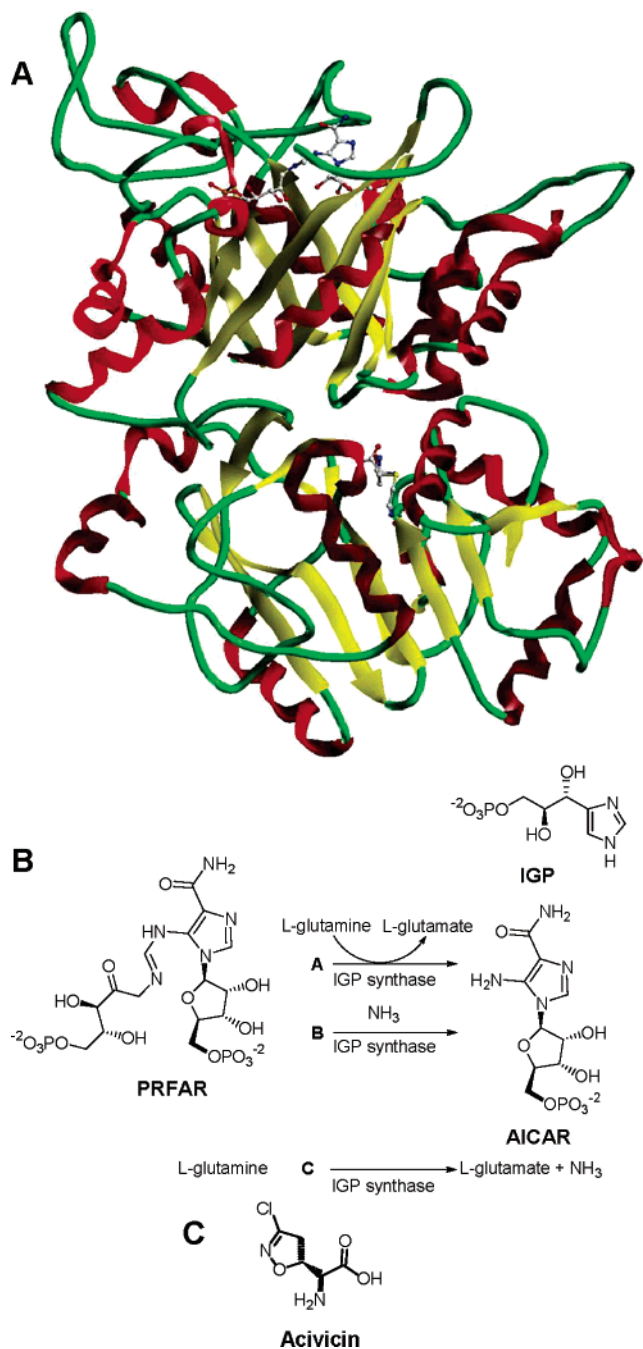


FIGURE 1: (A) Structure of *S. cerevisiae* IGP synthase. (B) Overall reactions. (C) Structure of the glutamine antagonist acivicin.

basis of comparison for nonfused heterodimeric systems from bacteria and lower organisms (3–5).

The triad amidotransferases have evolved to allow ammonia to be incorporated into a wide variety of substrates including amino acids, nucleotides, amino sugars, and coenzymes (2). The transfer of ammonia is unique within every triad glutamine amidotransferase protein (15), but all share the common feature that the resulting ammonia from glutamine hydrolysis is sequestered within the protein, away from the bulk solvent, and shuttled between the two active sites so that the reactivity of NH_3 is retained. A structural passage for ammonia is defined in IGP synthase and the hydrolysis of glutamine is tightly coupled with the binding of PRFAR. In IGP synthase, the binding of PRFAR stimulates glutaminase activity 4900-fold over the basal rate

(16). This general feature is a property of the other triad amidotransferases, although there are quantitative distinctions as to the degree of the glutaminase regulation (17–20). Our previous studies have shown that the entire PRFAR active site needs to be occupied for full glutaminase stimulation (16). Glutamine binding is not dependent upon PRFAR, but the commitment to glutaminase catalysis is affected by the acceptor substrate (i.e. the relative rate of the enzyme–substrate complex to proceed through the first irreversible step of ammonia formation reflected in changes of k_{cat}/K_M for the glutaminase half reaction induced by PRFAR binding). This is also seen in experiments using the irreversible glutaminase inhibitor acivicin (Figure 1) where the acivicin $k_{\text{inact}}/K_1^{\text{APP}}$ ($1100 \text{ M}^{-1} \text{ s}^{-1}$) with PRFAR is similar to the k_{cat}/K_m ($3100 \text{ M}^{-1} \text{ s}^{-1}$) of the stimulated glutaminase reaction (21). The nucleotide substrate PRFAR binds at the C-terminus of the $(\beta/\alpha)_8$ barrel with the two phosphates binding at opposite sides of the barrel opening. The structure of IGP synthase with PRFAR bound in a precatalytic state describes several protein–ligand interactions that could confer the binding signal to the glutaminase active site (8).

In this study, we have analyzed the interdomain contacts observed in the crystal structure of *S. cerevisiae* IGP synthase and identified a network of amino acids that mediate the PRFAR binding signal to the glutaminase active site. The amino acids, D359 from the cyclase domain, and K196, a residue adjacent to the glutaminase active site, form the only conserved interdomain salt bridge in the interface region. Through mutagenesis, kinetic and inhibition analysis, and molecular dynamics (MD) simulations, we have developed a theory of catalytic coupling and activation between the two active sites that may serve as a general mechanism for the entire triad glutamine amidotransferase family.

MATERIALS AND METHODS

Materials. All chemicals, buffers, resins, and enzymes were purchased from commercial sources. The plasmid, *pIGPS-T7*, was prepared as previously described (22). Phosphoenolpyruvate was synthesized according to a published procedure (23). *N*¹-[(5'-phosphoribosyl)-formimino]-5-aminoimidazole-4-carboxamide ribonucleotide (PRFAR) was synthesized according to a published procedure (16). Mutagenesis was performed as previously described (24). Custom oligonucleotides were synthesized commercially.

Site-Directed Mutagenesis. Oligonucleotides for site-directed mutagenesis were designed to include a restriction site to allow mutation verification by endonuclease digestion. All site-directed mutagenesis was carried out using *Pfu* Turbo DNA polymerase with direct mutation of the expressing plasmid (24). Confirmatory sequencing of the plasmids was performed by the Purdue Genomics Core Facility.

Protein Purification. Purification of his-tagged IGP synthase from *S. cerevisiae* was performed as previously described (3).

IGP Synthase Assays. Glutamine-dependent synthase activity assays were performed as previously described (22). Steady-state kinetic assays of IGP synthase activity in the presence of ammonium were performed in a 96-well UV-transparent plate with a final volume of 250 μL , containing 50 mM PIPES, pH 7.0, 0.5 mM EDTA, 400 mM NH_4Cl , and varying concentrations of PRFAR. Eight separate

readings for each concentration were analyzed, and the plates were read with a UV–Vis/fluorescence spectrophotometric plate reader. Steady-state kinetic assays of the glutaminase half-reaction or stimulated glutaminase (in the presence of substrate analogues or products) were performed according to an established procedure (16). Basal glutaminase activity was assayed using the same conditions as above except the IGP synthase reaction incubation time was increased to 1 h and 200 μ L aliquots were transferred to a 96-well untreated black flat-bottom plate. Glutamate concentrations were determined through the fluorescence of APADH (ex. 360 nm, em. 465 nm) (25) using standard curves prepared in parallel. Analyses of the reaction stoichiometry catalyzed by IGP synthase were performed as previously described (16).

Inhibition Analysis. Progress curves of IGP synthase mutants in the presence of substrates and the inhibitor acivicin were generated and analyzed by fitting to the following equations:

$$[P] = [P]_{\infty} (1 - e^{-A[I]t}) \quad (1)$$

and

$$A = \frac{k_{\text{inact}} \cdot K_a}{\left(1 + \frac{[S]}{K_m}\right) + K_a[I]} \quad (2)$$

where A is the apparent rate constant for the formation of the inhibited enzyme and K_a is the inhibitor association constant (26).

The assay contained 50 mM PIPES, pH 7.0, 100 μ M PRFAR, 5 mM glutamine, and varying amounts of acivicin (10–2000 μ M). The reaction was initiated by the addition of 1 μ M IGP synthase. Aliquots of 80 μ L were taken at varying time points. The amount of glutamate formed was determined by a coupling assay using glutamate dehydrogenase. Fifty millimolar Tris HCl, pH 8.0, 50 mM KCl, 1 mM EDTA, 0.5 mM 3-acetylpyridine adenine dinucleotide (APAD), and 5 μ g of glutamate dehydrogenase were added to each aliquot for a final volume of 250 μ L. The plate was incubated for 1.5 h at 37 °C with constant shaking (200 rpm). 200 μ L aliquots were transferred to a 96-well untreated black flat bottom plate. Glutamate concentrations were determined through the fluorescence of oxidation product, APADH (ex. 360 nm, em. 465 nm) (25) using standard curves prepared in parallel.

Simulations. The system setup and molecular dynamics (MD) simulations were similar to those previously described (6, 7). In the *S. cerevisiae* structure there are several areas of incomplete density at the top of the $(\beta/\alpha)_8$ barrel. Therefore, the crystal structure of the hetero-dimeric IGP synthase (hisH-hisF) complex isoform from *T. maritima* was used in all simulations because the structure is complete (PDB code: 1GPW) (4). The original *T. maritima* crystal structure had an active site mutation in the cyclase (his F) subunit (D11N), which we mutated back to its original, functional state. Chains C and D of the IGP synthase complex were chosen, as the loop on the c-terminal end of the cyclase subunit was in a closed and ordered conformation indicative of the active complex (7). The recently parametrized nucleotide substrate PRFAR, as well as the covalently bound glutamyl-thioester intermediate, was included in the simula-

tions (7). Both substrates were parametrized according to the CHARMM27 protocol (27–29).

Active site residues in both subunits were analyzed according to available biochemical information. For the glutaminase (hisH) subunit, H178 of the catalytic triad was deprotonated to be consistent with a covalently bound glutamine to C84 of the active site. The crystallographic waters within the protein and the subunit interface were kept in the simulation; no additional waters were added inside the protein or interface. After addition of hydrogens, the complex was solvated using the programs PSFGEN and SOLVATE through VMD (27, 31). The TIP3 water model was used for all water molecules (bulk and crystallographic); sodium ions were added to neutralize the system. The composite system was composed of 49 716 atoms; explicit solvent accounted for over 40 000 of these atoms. The complex was then minimized for 10 000 steps with the MD program NAMD2 (30); the CHARMM27 parameter set was used throughout the simulations (32).

The starting configuration of the protein complex (including all water molecules and both substrates) was equilibrated for 6 ns in the NPT ensemble using periodic boundary conditions and the Langevin Piston method to control pressure at 1 atm. The Particle Mesh Ewald method was employed to treat the electrostatic charge distributions without a cutoff (33). The system was equilibrated at 298.15 K with a time-step of 1 fs. No constraints were added to the system. Protein equilibration was determined by monitoring the RMSD of backbone atoms, as well as fluctuations in volume. The RMSD of the C_{α} atoms was approximately 1 Å at the end of the equilibration.

The wild-type structure was equilibrated for 6 ns before manual introduction of specific point mutations. The following mutations were made (*T. maritima* numbering first, yeast numbering in parentheses): N12A (N13A), K181A (K196A), D98A (D359A), and a double mutation D98A–K181A (D359A–K196A). Each mutation was subject to a short minimization and then equilibrated under identical conditions for at least 1 ns to observe interactions. Comparative dynamics to the wild type was used to ascertain effects of the mutations. The average equilibrium bond distances and dihedral values and their corresponding standard deviations (presented in Tables 4 and 5) were measured over the 1–3 ns dynamics simulation after initial transients disappeared. All runs were performed on either the National Center for Supercomputing Application's Platinum computer system (128-processors), or the Pittsburgh Supercomputing Center's Terascale system (128-processors), a local 128-processor SGI Origin 2000 cluster, or a local 27-processor Linux-i686-Scyld cluster. On these platforms each 1 ns trajectory took 12 h, 10 h, 1 d, or 3 d, respectively. In total, over 20 ns of simulation time were performed on the system.

RESULTS

Interdomain Salt Bridge Near the Glutaminase Active Site. The glutaminase active site resides at the interface of the two subdomains of IGP synthase. In the *S. cerevisiae* isoform the two domains are fused with the hinge region defined by a linker strand of 22 amino acids and a cation– π interaction between the C-terminus of the protein and an invariant glutaminase domain tryptophan near the linker

strand. The interactions between the two subdomains are mostly through backbone interactions between amine backbones of one subdomain and backbone carbonyls from the other. A hydrophobic patch is formed from the seventh and eighth beta strand of the glutaminase packing against the cyclase beta strands three, six, and seven (3). In the center of this subdomain contact region, a salt bridge is formed (Figure 2) between two invariant residues, D359 from the cyclase domain, and K196, a residue adjacent to two members of the catalytic triad of the glutaminase active site, H193 and E195. This interaction also includes an invariant residue from the glutaminase domain, N13. In all structures of IGP synthase (3–5), this salt bridge is intact despite the slight difference in orientation of the two subdomains. In one structure, for example, the angle of interaction between the two subdomains is 15°. D359 resides at the N-terminus of β 4, part of the internal beta sheet making up the $(\beta/\alpha)_8$ barrel. This beta strand stretches the length of the cyclase domain to interact at one of the phosphate binding regions in the PRFAR active site (Figure 2). The proximity of the D359-K196 interaction near the glutaminase active site, and its structural connectivity with the PRFAR active site, formed a basis for probing the functional roles of these interactions through site-directed mutagenesis.

Five Kinetic Assays To Assess Changes in Protein Function. The overall reaction of IGP synthase involves glutamine hydrolysis, ammonia transfer, and incorporation into the PRFAR substrate. Glutaminase activity in the presence and absence of PRFAR indicates the degree of stimulation as a function of binding in the cyclase active site or changes in the competency of the glutaminase active site. PRFAR turnover can be analyzed using glutamine or ammonia as the nitrogen source. Ammonia transfer is assessed by measuring the overall stoichiometry of the two half reactions and analyzing the formation of products. In wild type, the ratio of PRFAR turnover to the consumption of glutamine is unity. Therefore, any changes in stoichiometry would indicate an uncoupling of the two catalytic sites.

D359: The Cyclase Component of the Interdomain Salt Bridge. Mutation of D359 to alanine significantly altered the capacity of PRFAR binding to stimulate glutaminase activity (Table 1). The basal level glutaminase activity in the absence of PRFAR is similar to wild type basal levels while the stimulated activity is slightly greater than the basal level. This effect is also revealed in the glutamine-dependent turnover of PRFAR (Table 2). Turnover of PRFAR is reduced with a commitment factor 2300-fold lower than wild type while only showing a 2-fold effect on the ammonia-dependent reaction (Table 2). The stoichiometry of 2:1 for the hydrolysis of glutamine and the turnover of PRFAR also indicates a moderate uncoupling of the two active sites (Table 1). The lack of PRFAR stimulation is consistent with reduced turnover kinetics of the nucleotide substrate and demonstrates that D359 is an integral member of the PRFAR binding-signal that activates the glutaminase active site.

K196: The Interacting Residue Adjacent to the Glutaminase Catalytic Triad. The K196 residue is proximal to the glutaminase active site and bridges to the cyclase domain interacting with D359. Mutation to alanine was pursued to remove the interacting residue. In the glutaminase half reactions, the protein exhibited 10-fold and 4-fold enhancements of glutamine commitment (Table 1); a result not

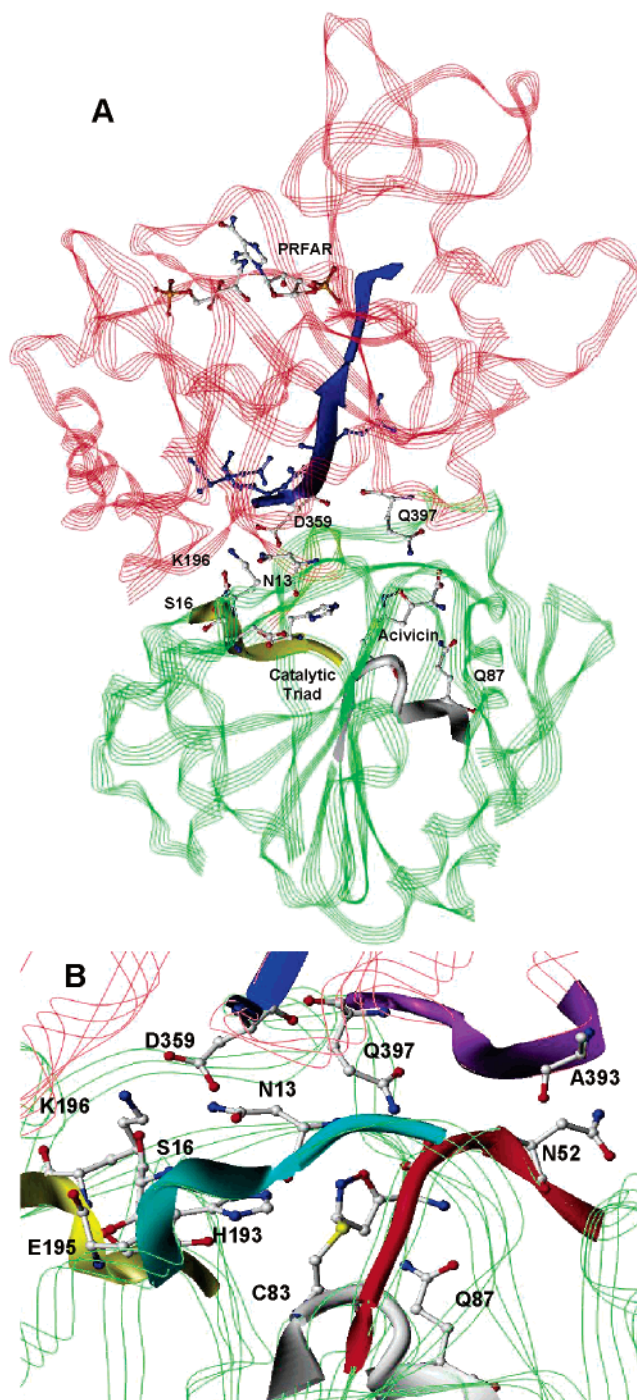


FIGURE 2: A network of interdomain interactions stabilizes the overall architecture of the glutaminase active site. (A) The glutaminase and PRFAR active sites are directly connected through beta-strand $f\beta 4$ highlighted in solid blue. (B) Closeup of interdomain region: the first residue of $f\beta 4$ (D359) forms a key salt bridge interaction with K196 of the glutaminase loop (shown in solid yellow with H193 and E195). The nearby helix composed of residues 9–13 (presented in cyan, N13, S16) forms several hydrogen bonds with the interdomain salt bridge. Other regions of interest are the nucleophilic elbow (presented in solid white and including C84, Q87), the oxyanion strand (in solid red with N52) and the cyclase loop (in solid purple with Q397 and A393).

observed for any other mutation to date. The consequences on the PRFAR turnover kinetics were largely unaffected. However, the differences in the k_{cat}/K_m for the PRFAR-stimulated glutaminase half reaction and the glutamine-dependent PRFAR turnover are consistent with an uncou-

Table 1: IGP Synthase Glutaminase Kinetic Parameters

mutation	K_m , basal ^a (mM)	k_{cat} (s ⁻¹)	k_{cat}/K_m (M ⁻¹ s ⁻¹)	k_{cat}/K_m WT/ mutant	K_m , half-reaction ^b (mM)	k_{cat} (s ⁻¹)	k_{cat}/K_m (M ⁻¹ s ⁻¹)	k_{cat}/K_m stimulated/ basal	stoichiometry ^c glutamate/ IGP
wild type	4.7 ± 0.2	5.5 ± 0.1 × 10 ⁻³	1.18 ± 0.06		1.2 ± 0.1	6.8 ± 0.2	5.8 ± 0.8 × 10 ³	4900	1:1
N13A	6.2 ± 0.9	1.4 ± 0.3 × 10 ⁻³	0.23 ± 0.06	5	5 ± 1	0.1 ± 0.03	23 ± 7	100	8:1
K196A	1.72 ± 0.04	2.1 ± 0.1 × 10 ⁻²	12.7 ± 0.6	0.1	0.44 ± 0.02	9.8 ± 0.2	2.5 ± 0.1 × 10 ⁴	2000	9:1
D359A	1.4 ± 0.2	7.8 ± 0.3 × 10 ⁻⁴	0.55 ± 0.08	2	4.2 ± 0.2	0.004 ± 0.001	1 ± 0.3	2	2:1
K196A/D359A	1.6 ± 0.3	3 ± 1 × 10 ⁻³	2.2 ± 0.8	0.5	0.5 ± 0.04	0.209 ± 0.003	3.9 ± 0.3 × 10 ²	180	110:1
Q397A	8.3 ± 0.8	1.8 ± 0.2 × 10 ⁻³	0.22 ± 0.03	5	2.5 ± 0.6	1.1 ± 0.1	4.5 ± 1 × 10 ²	2000	2:1

^a Reaction C in Figure 1. Glutamine hydrolysis in the absence of PRFAR. ^b Reaction A in Figure 1. Glutamine was the varied substrate and the concentration of PRFAR was constant at 100 μM. ^c Assay contained 100 μM PRFAR, 5 mM glutamine.

Table 2: IGP Synthase Cyclase Kinetic Parameters

mutation	K_m , PRFAR ^a (Gln) (μM)	k_{cat} (s ⁻¹)	k_{cat}/K_m (M ⁻¹ s ⁻¹)	k_{cat}/K_m WT/mutant
wild type	5 ± 1	5.4 ± 0.5	1.2 ± 0.2 × 10 ⁶	
N13A	1.3 ± 0.4	1.12 ± 0.08 × 10 ⁻²	9 ± 3 × 10 ³	130
K196A	0.27 ± 0.02	0.74 ± 0.01	2.8 ± 0.2 × 10 ⁶	0.43
D359A	5.5 ± 0.9	2.9 ± 0.2 × 10 ⁻⁴	5.2 ± 0.9 × 10 ²	2300
K196A/D359A	14.1 ± 0.3	7.0 ± 0.3 × 10 ⁻³	5.1 ± 0.1 × 10 ²	2300
Q397A	3.6 ± 0.4	0.56 ± 0.02	1.6 ± 0.2 × 10 ⁵	7.5
mutation	K_m , PRFAR ^b (NH ₄ ⁺) (μM)	k_{cat} (s ⁻¹)	k_{cat}/K_m (M ⁻¹ s ⁻¹)	k_{cat}/K_m WT/mutant
wild type	55 ± 8	0.845 ± 0.007	1.5 ± 0.2 × 10 ⁴	
N13A	71 ± 7	0.35 ± 0.03	4.9 ± 0.6 × 10 ³	3
K196A	34 ± 3	0.46 ± 0.05	1.4 ± 0.2 × 10 ⁴	1
D359A	109 ± 3	0.39 ± 0.01	3.6 ± 0.2 × 10 ³	4
K196A/D359A	26 ± 1	0.11 ± 0.03	3.8 ± 0.8 × 10 ³	4
Q397A	30 ± 6	0.38 ± 0.03	1.2 ± 0.3 × 10 ⁴	1
mutation	K_m , Gln ^c (mM)	k_{cat} (s ⁻¹)	k_{cat}/K_m (M ⁻¹ s ⁻¹)	k_{cat}/K_m WT/mutant
wild type	1.8 ± 0.2	6.9 ± 0.3	3.8 ± 0.4 × 10 ³	
N13A	4.8 ± 0.9	1.9 ± 0.02 × 10 ⁻²	4 ± 0.8	950
K196A	0.49 ± 0.04	0.6 ± 0.01	1.2 ± 0.1 × 10 ³	3
D359A	14 ± 1	5.9 ± 0.2 × 10 ⁻³	0.42 ± 0.04	9000
K196A/D359A	2.3 ± 0.3	7 ± 2 × 10 ⁻³	3.2 ± 0.9	1000
Q397A	7 ± 1	1.4 ± 0.2	2.1 ± 0.3 × 10 ²	18

^a Reaction A in Figure 1. PRFAR was the varied substrate and the concentration of glutamine was constant at 40 mM. ^b Reaction B in Figure 1. PRFAR was the varied substrate and the concentration of NH₄⁺ was constant at 400 mM. ^c Reaction A in Figure 1. Glutamine was the varied substrate and the concentration of PRFAR was constant at 100 μM.

pling of the cyclase and glutaminase functions (Tables 1 and 2). The stoichiometry reflected this 10-fold effect, with a glutamine hydrolysis to PRFAR turnover ratio of 9:1. The increase in basal glutaminase commitment factor over wild type indicated an enhanced competency of the active site for glutamine turnover in the absence of PRFAR substrate while not impacting the substrate binding signaling event from the cyclase domain. However, the lack of interaction across the interface does have a consequence on the efficiency of ammonia transfer indicated by the altered stoichiometry of the amidotransfer process.

A Double Mutation at Position 196 and 359. As a check of the distinct roles for each interface residue, a double mutant K196A and D359A was created. As expected from the single D359 mutant, the PRFAR commitment factor was reduced 2300-fold from wild type, while the impact on the ammonia-dependent activity was minimal (Table 2). A striking result with the double mutant was the fact that the basal glutaminase was similar to wild type and could be stimulated by PRFAR binding 180-fold unlike the D359A mutant (Table 1). The stoichiometry of the two half-reactions is uncoupled in this mutant with over 100 glutamine equivalents hydrolyzed for every PRFAR turnover. This result shows that the glutaminase active site is still competent

and able to catalyze the hydrolysis reaction, but the resulting ammonia is not efficiently channeled through the protein to the awaiting PRFAR due to the alterations at the domain interface. Furthermore, the fact that the PRFAR-dependent stimulation has been partially restored in the double mutant implicates a role for K196 in down regulating the glutaminase active site.

N13: A Glutaminase Residue Interacting with the Interdomain Salt Bridge. This glutaminase domain N13 interacts with D359 on the cyclase domain through hydrogen-bonding of the asparagine carboxamide group and the carboxylate side chain of aspartic acid. Mutation of N13 to alanine produced an enzyme with PRFAR-dependent stimulation of the glutaminase half reaction that was only 100-fold over the basal level indicating a reduced capacity for PRFAR binding to signal to the glutaminase site (Table 1). As expected, the impact of this interface mutation is minimal on the ammonia-dependent PRFAR turnover but the impaired signaling to the glutaminase site also is reflected as a 130-fold reduction of the glutamine-dependent amidotransfer (Table 2). As seen with the other interface mutations, the lack of the asparagine side chain between the two domains also impacts the efficiency of ammonia transfer since the overall reactions are uncoupled as seen in the stoichiometry

Table 3: Acivicin Inactivation

mutation	K_I (μM)	k_{inact} (s^{-1})	k_{inact}/K_I ($\text{M}^{-1}\text{s}^{-1}$)	k_{inact}/K_I WT/mutant
wild type	6 ± 1	$1.6 \pm 0.1 \times 10^{-3}$	$2.9 \pm 0.6 \times 10^2$	
N13A	46 ± 7	0.14 ± 0.02	$2.9 \pm 0.7 \times 10^3$	0.1
K196A	38 ± 8	$2.8 \pm 0.2 \times 10^{-2}$	$7 \pm 2 \times 10^2$	0.4
D359A	$4 \pm 2 \times 10^2$	$5.0 \pm 2 \times 10^{-6}$	$1.3 \pm 0.9 \times 10^{-2}$	20000
K196A/ D359A	52 ± 5	$1.7 \pm 0.4 \times 10^{-2}$	$3.3 \pm 0.8 \times 10^2$	1
Q397A	$4 \pm 1 \times 10^3$	$1.5 \pm 0.5 \times 10^{-4}$	$4 \pm 2 \times 10^{-2}$	7000

for glutamine equivalents hydrolyzed per PRFAR turnover of eight.

Q397: A Cyclase Domain Residue Stabilizing the Bound Intermediate. In previous studies of IGP synthase from *E. coli*, a glutamine at the cyclase position 397 (hisF Q123 in *E. coli*) when mutated to arginine was shown to disrupt the glutaminase activity of the protein (35, 36). In the crystal structures of the *S. cerevisiae* isoform, this glutamine is seen to interact with the bound glutamine antagonist acivicin in the glutaminase active site, stabilizing the α -amino acid moiety of the inhibitor in conjunction with Q87 from the nucleophilic elbow (containing the catalytic cysteine). We speculated that the bulky side chain substitution (Q397R) occluded the active site and prohibited the binding of the substrate glutamine. In these studies, we analyzed the role of the Q397 residue from the cyclase domain by mutation to alanine. The loss of this side chain did impact the basal glutaminase but not the capacity of PRFAR-binding to stimulate glutaminase (Table 1). A moderate degree (2:1) of uncoupling of the amidotransfer process was also detected for this mutant. The role of the Q397 in the binding specificity for glutamine is reflected in the PRFAR turnover where an 8-fold reduction in k_{cat}/K_m is observed (Table 2).

Inhibition Studies To Assess Forward Commitment to Glutamine Hydrolysis. In previous studies we determined that the inactivation kinetics of acivicin in the glutaminase active site of IGP synthase and other triad glutamine amidotransferases mimicked the forward commitment to glutamine hydrolysis (21). This compound is a competitive glutamine antagonist that undergoes covalent addition to the active site C83 in the *S. cerevisiae* IGP synthase. To further assess the roles of the interface residues identified, we followed the rate of formation for glutamate in the presence of PRFAR and acivicin as an approach to gain further mechanistic information regarding each of the key interface amino acid residues under consideration.

The D359A mutation had a profound impact on the acivicin inactivation of the enzyme with k_{inact}/K_I decreased 20 000-fold over wild type (Table 3) with the effect primarily in k_{inact} , where the rate measured was near the threshold of detection at $5 \times 10^{-6} \text{ s}^{-1}$. This result is in contrast to the K196A mutation, which had a minimal impact on the overall kinetics of acivicin inactivation. The rate of the covalent modification in the K196A mutant occurs more rapidly as seen by 18-fold enhancement of k_{inact} (Table 3). The K_I of this mutant was increased 6-fold to render a 2.5-fold enhancement of the k_{inact}/K_I . A similar increase in the k_{inact} was observed for the K196A/D359A double mutant, and in this case the overall effect on k_{inact}/K_I was unchanged from the wild-type enzyme. The N13A mutant showed an enhancement of the inactivation with acivicin for both k_{inact}

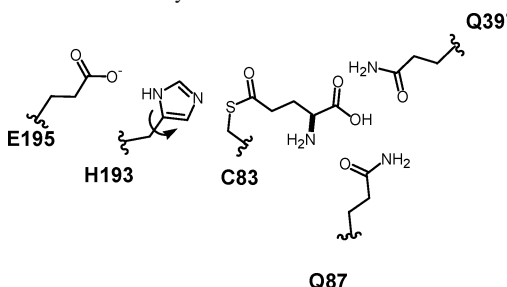
(90-fold increase) and k_{inact}/K_I 2900 $\text{M}^{-1} \text{ s}^{-1}$ (10-fold increase), indicating a greater forward commitment to inhibition. In total, the inactivation kinetics of the mutants of IGP synthase are consistent with the changes in the data provided in Tables 1 and 2. The loss of function of the D359 position renders the cyclase domain unable to signal the PRFAR binding event to the glutaminase active site. In addition, the D359A mutant exerts an inhibitory effect on the glutaminase function as evidenced by the drastic decrease in stimulated glutaminase. Removal of the hydrogen bonding pairs on the glutaminase domain (K196 and N13) restores glutaminase function and does not impair the acivicin addition reaction. These residues are not likely to be involved in the catalytic function of the glutaminase site but have a regulatory role that requires coordination with D359 for proper orientation.

The acivicin inactivation kinetics with the Q397A mutant demonstrated a high degree of resistance to inhibition as reflected in both an increased K_I (700-fold) and a decreased k_{inact} (10-fold). As proposed, these data are also consistent with those in Tables 1 and 2 and further indicates the proposed role in providing binding specificity to the glutamine binding site.

Molecular Dynamics Simulations of IGP Synthase. Although the kinetic and inhibition analyses described in this study were performed with the *S. cerevisiae* isoform of IGP synthase, we chose to use the *T. maritima* isoform in our MD simulations. The crystal structure of this protein was more complete than that of *S. cerevisiae*, which has several areas of incomplete density at the C-terminus of the $(\beta/\alpha)_8$ barrel. A difference in the relative orientation of the two subdomains in the two structures prompted a determination of the rmsd for the two isoforms by analyzing each subdomain separately. Within the glutaminase active site, the rmsd of the catalytic triad is 0.9 Å. The structural overlaps of the glutaminase and synthase domains are within 1.86 Å and 1.57 Å, respectively. In addition, the structural similarity between the two isoforms has been established in (8). An extensive comparison of both sequence and structure similarities is provided as Supporting Information to this paper. A more detailed description of the interface is provided in (38).

Wild Type. As a baseline for comparison with the mutant systems, the dynamics of the wild type simulations were used to determine the time-averaged equilibrium bond distances, dihedral fluctuations, and local interactions. The network of key wild type active site interactions is shown in Figure 2B and 3A. In the wild type simulation, the delta nitrogen of H193, which is the nitrogen closest to E195, forms a tight hydrogen bond with E195 of the triad. K196 and D359 form a strong salt bridge that is never broken at any point during the simulations. The side chain of N13 interacts closely with the residue at position 16, which is a serine or asparagine in all available sequences. Most notably, all of the local hydrogen bond and salt bridge interactions of interest exhibit low values of deviation throughout the simulation. By comparison, hydrogen bond distances between E195 and H193 for the single mutants increased, indicating movement in the imidazole ring of H193 (Table 4). As an additional measure of active site flexibility, the dihedral angle about the H193 imidazole ring (CA–CB–CG–ND) was monitored throughout the simulations. In wild type, the stable network

Table 4: of Residue Interaction Distances and Rotational Analyses



	bond length (Å) ^a					H193 dihedral CA–CB–CG–ND (deg) ^b	position 13	
	C83–H193	D359–H193	E195–H193	K196–D359	K196–E 195		phi ⁱ ^b	psi ^b
wild type	4.0 (0.3)	6.8 (0.3)	2.9 (0.1)	2.7 (0.1)	5.7 (0.4)	88.9 (9.2)	–80.0 (10.6)	111.1 (10.7)
N13A	3.9 (0.5)	6.1 (0.5)	3.6 (0.7)	2.7 (0.1)	6.0 (0.6)	95.0 (88.3)	–80.8 (12.3)	88.5 (23.7)
K196A	3.7 (0.3)	5.0 (0.3)	3.7 (0.6)	n.a.	n.a.	118.5 (37.3)		
D359A	3.6 (0.3)	n.a.	4.2 (0.5)	n.a.	2.7 (0.2)	125.3 (45.8)		
K196A/D359A	3.8 (0.3)	n.a.	3.0 (0.2)	n.a.	n.a.	92.3 (11.5)		
Q397A	3.8 (0.4)	6.5 (0.7)	4.6 (0.6)	2.8 (0.1)	4.6 (0.4)	67.3 (131.8)		

^a The average bond lengths are reported with standard deviation in parentheses and are shown in Figure 3. ^b The average angles are presented with standard deviation in parentheses.

of interactions within the glutaminase active site causes the histidine of the catalytic triad to be rigidly held, as indicated by the minimal dihedral fluctuation of 9.2° (Table 4) The structural stabilization, provided by the extensive hydrogen bond and salt bridge network of interactions within the glutaminase active site could account for the enzyme's strong catalytic competence as observed experimentally.

D359A. This mutant results in the loss of a salt bridge partner for K196. It is clear from the MD simulations that K196 can now adopt an alternate rotamer conformation (Figure 3B). In the absence of D359, the amine group of K196 forms a salt bridge with the carboxyl group of E195 (Table 4). Furthermore, this new salt bridge between K196 and E195 compromises the hydrogen bond interaction between E195 with H193 (Table 4). This local structural change pulls H193 out of plane with the catalytic cysteine, allowing large fluctuations of the H193 imidazole ring dihedral angle (Table 4) We propose that the increased flexibility of H193 could account for the decreases observed in the catalytic competence of the glutaminase active site.

K196A. In the wild type simulation, residues K196 and D359 form a critical salt bridge, which, in addition to being an important signaling element, also supports the structure and stability of the glutaminase active site. Without K196, D359 loses its natural salt bridge partner and formed a new hydrogen bond interaction with the active site histidine (Figure 3C). In this simulation, H193 mutually interacts with two adjacent negatively charged groups: D359 and E195 rather than a single interaction with D359 as observed in the wild type. These two residues adopt equally close proximity to the hydrogen on the delta nitrogen of H193. The additional hydrogen bond partner could therefore partially compensate for the lost salt bridge, and, although the flexibility of the histidine dihedral of interest is increased from wild type (Table 4), it still allows H193 to function as a general base to the catalytic cysteine. Ultimately, this mutant retained a catalytically competent glutaminase active site, as indicated by the experimental results.

N13A. In the wild type system, on one side of the glutaminase active site, N13 and S16 formed close interac-

tions. Though they did not directly interact with H193, they are part of a helix forming one of the walls of the glutaminase active site and were expected to play an important role in stabilizing the architecture of the active site. The MD simulations indicate that the mutation of asparagine to alanine at position 13 disrupts the interactions of S16 with D359 (Figure 4). Overall, the glutaminase active site demonstrates increased motion, as indicated by (i) the larger fluctuations in the imidazole ring dihedral angle of H193 (Table 4), (ii) an increase in the degrees of freedom for the phi-psi bonds at position 13, and (iii) greater deviations in the equilibrium bond lengths for all of the key interactions in the active site (Table 4). These results indicate that N13 plays a key role in stabilizing (i.e. providing structural rigidity to) the overall architecture of the glutaminase active site.

K196A/D359A. In the simulations of this double mutant it was found that H193 optimizes its position so that the exchangeable proton at the delta nitrogen of the imidazole ring forms a hydrogen bond with the charged group of E195. The loss of both members of the interdomain salt bridge allows H193 and E195 to adopt the proper catalytic orientation for glutamine hydrolysis (Figure 3), with minimal fluctuation of the histidine imidazole ring dihedral (Table 4). This is consistent with the observed catalytic competence of the glutaminase domain, albeit with a reduced stoichiometry (Table 1). Interestingly, the MD simulations indicate that the loss of this salt bridge opens another cavity within the interface that is more distant from the mouth of the (β/α)₈ barrel of the synthase subdomain. The ammonia molecule, which normally diffuses inside the interface during the equilibration, was observed to enter this new cavity and remain there for over 1 ns. Extended simulations (for an additional 4 ns) show that the ammonia does not diffuse out of this cavity into the bulk solvent, nor do any additional bulk water molecules enter the sequestered ammonia chamber; however, the additional diffusive motion experienced by ammonia in the *K196A/D359A* mutant may explain the uncoupling of the two reactions as indicated by the disrupted stoichiometry of 110:1 (Table 1).

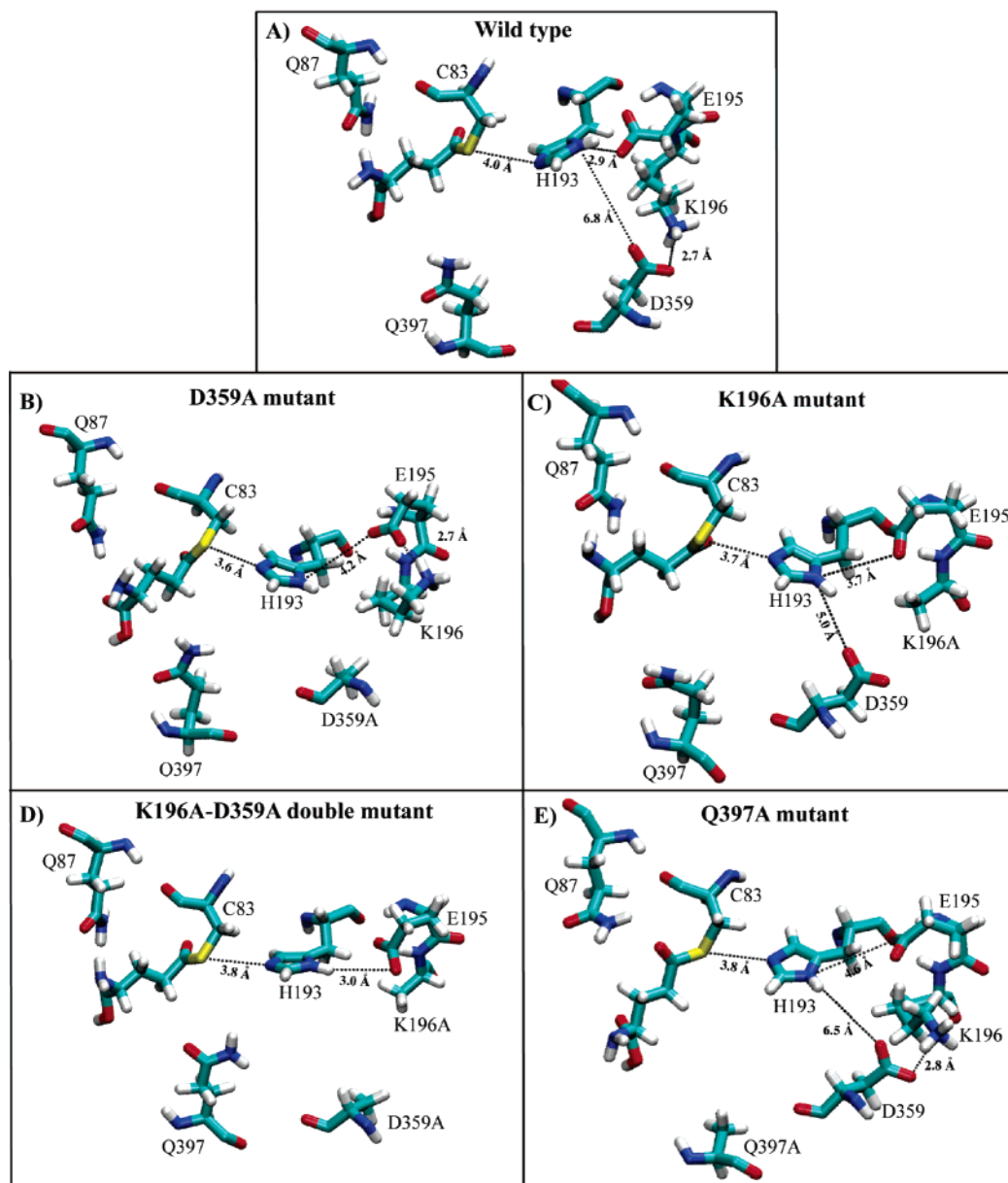


FIGURE 3: Representative snapshots of the glutamyl-thioester intermediate in the glutaminase active site from the MD trajectories are presented for each mutant system. Equilibrium bond distances of interest are denoted with average values, as determined from the trajectories.

Q397A. Previous experimental results indicated that this residue was critical for substrate recognition (1, 3). In wild-type MD simulations, the glutamyl-thioester intermediate interacts with both Q397 and Q87 from the nucleophilic elbow. With the loss of Q397, the intermediate dissociates from Q87, shifting from a close interaction of 3.1 Å to 6.7 Å (Table 5). Interestingly, the loss of this cyclase glutamine affects the interaction between E195 and H193; the hydrogen bond lengthens to 4.6 Å from 2.9 Å in wild type (Table 4). The rigidity of the histidine ring is also significantly compromised (Table 4). These simulations were consistent with the experimental results for the Q397A mutants, and all indicate a direct role in the specificity of the glutamine binding site.

DISCUSSION

Interdomain Contacts and Glutaminase Activation. IGP synthase is an excellent model for the study of the triad glutamine amidotransferases in that the interdomain contacts

are well described in the crystal structures of the yeast isoform (3, 8). Of all the interactions across the two subdomains there is only one conserved salt bridge, and it is adjacent to the glutaminase active site. The crystal structure and MD simulations indicate that the K196-D359 salt bridge does not form the outer edge of the protected ammonia cavity (chamber I in ref 38); therefore, mutation does not allow bulk solvent immediate access to the chamber. MD simulations of the double mutant, K196A/D359A, show that no additional water molecules enter the cavity during the six ns equilibration. However, as the K196-D359 salt bridge participates in the stabilization of the interface, it is possible that loss of this salt bridge in the double mutant affects the “breathing motion” between the two subdomains. Destabilization could cause the interface to open more frequently or for prolonged periods of time, which could result in loss of ammonia to the bulk solvent and therefore explain the 110:1 disruption in stoichiometry. Unfortunately, the breathing motion would require large-scale motions of the domains,

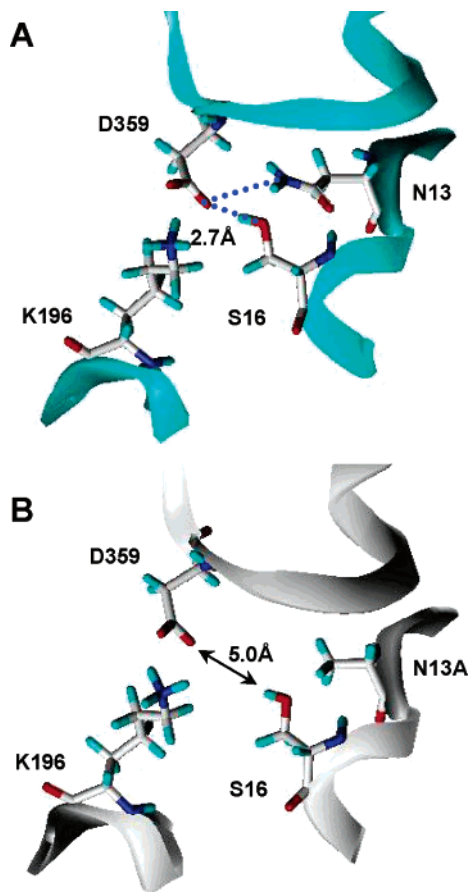


FIGURE 4: A representative snapshot from the MD trajectory of the N13A mutation shows that the loss of the carboxamide side chain interaction with D359 affects the S16–D359 hydrogen bond interaction and architecture of the glutaminase active site. (A) The conformation in wild-type indicates a stable hydrogen bond between the S16 hydroxy group and D359. (B) The loss of this hydrogen bond in the N13A system increases the overall flexibility of the active site and shifts the nearby helix away from the key interdomain salt bridge.

Table 5: Bond Distances (Å) of Glutamyl Thioester to Binding Residues^a

	O1 γ –Q87:N2 ϵ	N γ –Q87:O1 ϵ	O2 γ –Q397 O1 ϵ	O1 ϵ –Q397:N2 ϵ
wild type	3.4 (0.4)	3.1 (0.4)	7 (1)	8.8 (0.7)
K196A	3.4 (0.4)	3.2 (0.6)	4.3 (0.7)	6.6 (0.7)
K196A/ D359A	3.3 (0.4)	3.3 (0.6)	3.8 (0.4)	5.4 (0.4)
Q397A	3.6 (0.4)	6.7 (0.7)	n.a.	n.a.

^a The average bond lengths are reported with standard deviation in parentheses.

which is beyond the scope of the equilibrium MD simulations presented here. The breathing motion at the interface is more clearly seen in ref 37, where simulations of PRFAR undocking result in large-scale hinge-opening motions between the two subdomains. Mutations of the residues in this salt bridge altered the activity of the protein, such that in one mutation, D359A, the glutaminase activity in the presence of PRFAR was equivalent to the basal (negligible) glutaminase rate of the wild-type protein. The loss of PRFAR stimulation in this mutant confirms a key role for D359 as an interdomain contact that regulates the overall efficiency of the glutaminase active site through a direct interaction with K196. The MD simulations also show that the D359A

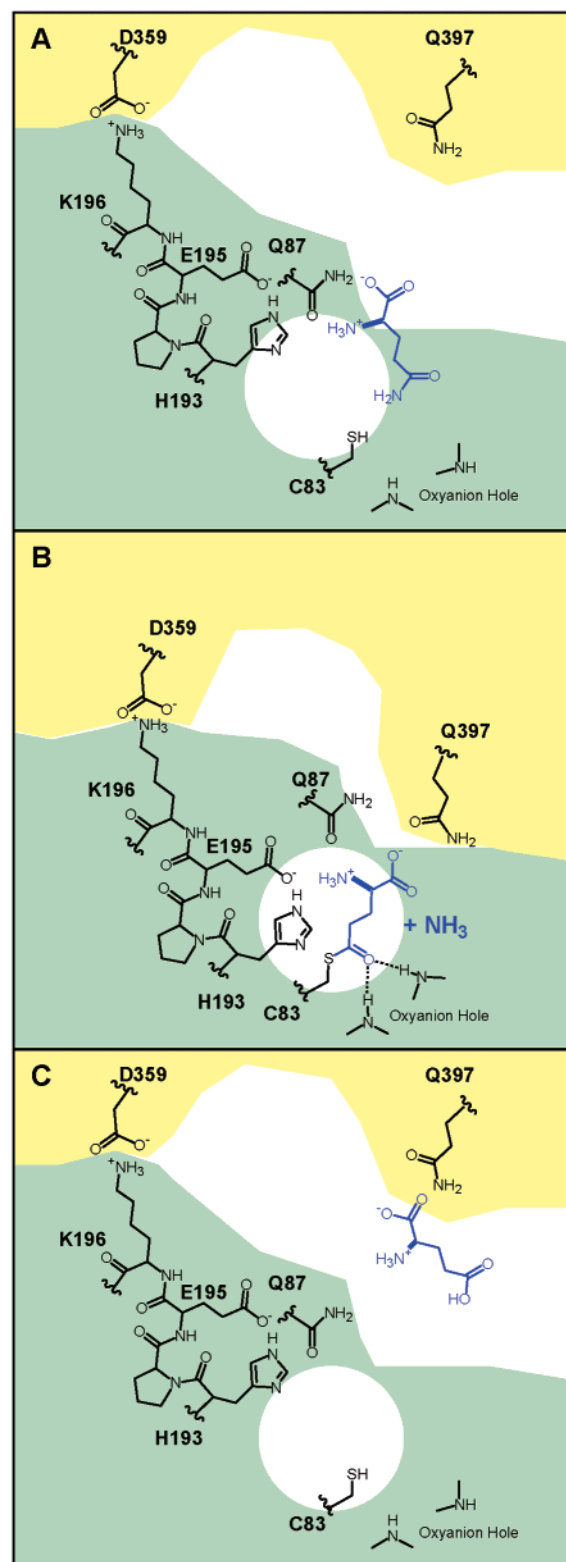


FIGURE 5: A series of schematics depicting the proposed dynamics within the glutaminase active site, induced upon PRFAR binding, are presented. The cyclase domain is shaded in yellow and the glutaminase domain in green. (A) Initially, the glutaminase substrate (in blue) enters active site with an orientation near Q87 and the oxyanion hole is not formed. (B) PRFAR binding initiates a tightening of the interface, which assists in the formation of the oxyanion hole. The glutamine substrate is now properly oriented by Q87 and Q397, and D359 pushes the catalytic triad into its catalytically competent conformation. The thioester intermediate is formed, and NH₃ is subsequently released. (C) Relaxation of the protein causes the interface region to open, expelling the glutamate product (in blue).

Table 6: Residues in Other Triad Glutamine Amidotransferases Proposed to Function in Glutaminase Stimulus Signaling Across the Subdomain Interface^a

	organism	catalytic triad	proposed residues involved in signaling		
			glutaminase	acceptor domain	acceptor active site
IGP synthase	<i>S. cerevisiae</i>	C83, H193, E195	K196	D359	T365
anthranilate synthase	<i>S. solfataricus</i>	C84, H175, E177	S178	D275	D266
CTP synthetase	<i>E. coli</i>	C379, H515, E517	S520	H314	D303
FGAR-amidotransferase	<i>S. typhimurium</i>	C1135, H1260, E1262	R1263	D657	E648

^a Carbamoyl phosphate synthetase (CPS) and GMP synthetase (GMPS) are not included in this table for the following reasons: The interface in CPS includes an additional N-terminal domain that introduces an additional level of complexity into the domain interactions. The crystal structure of GMPS indicates an inactive form of the protein with the glutaminase active site exposed to bulk solvent and not interacting with the acceptor domain.

mutation allowed K196 to shift and interact with the catalytic glutamic acid, changing the rotamer state of both E195 and H193. The shift of K196 to the glutaminase active site is consistent with the structural data for the *T. maritima* glutaminase (hisH) in the absence of the cyclase (hisF) (39). In this structure, K196 has no pairing partner from the cyclase domain and folds down into the glutaminase active site, altering the backbone rotation of the loop containing the two members of the catalytic triad and rendering the enzyme inactive. Therefore, the interdomain contacts serve as a conduit for transduction of the PRFAR binding information by direct activation of the glutaminase catalytic site.

From the crystal structure of the yeast IGP synthase, K196 draws the glutaminase loop (containing H193 and E195) away from the catalytic cysteine, preventing H193 from functioning as a general base to the cysteine. This structural interpretation is consistent with the results of the K196A mutant where a 10-fold enhancement of the basal glutaminase activity of the protein was observed. Furthermore, the enhanced catalytic competence of the glutaminase active site in the K196A mutation was revealed by an enhanced forward commitment (covalent addition) to acivicin inactivation. In simulations of this mutation, without its amine electrostatic partner, D359 was able to interact with H193, stabilizing this residue further in its active catalytic conformation. From these data we propose that K196 acts as a regulatory side chain to (i) deactivate the glutaminase active site when the domain is not docked to the cyclase domain and (ii) pull the loop containing H193 and E195 away from C83 until PRFAR is bound to IGP synthase.

Two other residues interact with the interdomain salt bridge, N13 and S16. The carboxamide function (N13) is conserved at this location throughout the triad glutamine amidotransferase family and provides a key interaction with the glutaminase loop containing the catalytic histidine and glutamic acid residues. From the studies presented here, mutation of this asparagine to alanine decreased the PRFAR-dependent glutaminase stimulation and altered the coupling of the two half-reactions. A structural explanation of this effect is offered by the MD simulations which reveal that the loss of the carboxamide side chain at N13 structurally destabilizes the alpha helix containing residues 9 to 16, which forms one of the walls of the glutaminase active site. The partial unfolding of the small helix is seen in changes in the phi-psi angle and distances reported in Table 4 and Figure 4B. Furthermore, the loss of the carboxamide side chain also disrupts the S16–D359 hydrogen bond interaction and markedly increases the flexibility of the active site histidine (Table 4). Taken together, the N13A mutation appears to

structurally destabilize the glutaminase active site. Yet, this altered architecture still allows the active site to remain catalytically competent, resulting in increased glutamine hydrolysis relative to IGP production.

The role of Q87 (invariant across the family of triad GATs) as a critical residue in glutamine hydrolysis has been well established (40, 41). Another interdomain contact residue Q397 appears to function in cooperation with Q87 to confer specificity to the glutaminase substrate binding site. While Q397 is not essential for the glutaminase activity, the evidence from the acivicin inactivation studies indicates that the residue is critical for optimal binding orientation. In previous studies, we determined that acivicin was an excellent substrate mimic of glutamine (Figure 1c), even though the molecule contains a heterocycle that constrains the orientation of the α -amino acid recognition components (21). Acivicin displays reactivity equivalent to the substrate glutamine in IGP synthase, but the absence of the glutamine side chain of Q397 had a significant impact on the ability of the inhibitor to bind with appropriate alignment of reactive groups. These results are also consistent with previous studies of the Q397R mutant that was also found to have lost the capacity to utilize glutamine as a substrate (36). The proposed interaction of the substrate or substrate mimic with the side chain of Q397 helps to properly orient the molecule allowing it to bind Q87 and enhances the commitment to catalysis. This interaction is cooperative and dependent upon the binding of the PRFAR in the cyclase active site.

In addition to the nucleophilic elbow interaction at Q87, the bound glutamine intermediate is stabilized by an oxyanion hole (42) that forms from the helix dipole at V84 (adjacent to the catalytic cysteine 83) and G50 of a strand forming the wall of the active site (21, 43). This region of the structure has been called the oxyanion strand (3) denoting its role in formation of the intermediate-stabilizing oxyanion hole. In the *S. cerevisiae* structure of IGP synthase, the nitrogen of G50 is pointing away from the catalytic cysteine and the oxyanion hole is collapsed. In other triad GAT structures, the oxyanion hole is oriented for interaction with the glutamine carboxamide group and the oxyanion strand maintains an interdomain contact several residues downstream from the oxyanion hole. In IGP synthase, this interdomain contact appears transient, forming between the amino group of glutaminase residue N52 and the carbonyl of cyclase A393 only when the two subdomains form a tight complex (Figure 2) (3). Structural studies of the chymotrypsin-like proteinase arterivirus nsp4 have shown that the oxyanion hole in this enzyme is also collapsed, but forms when the substrate is bound (44). Stabilization of the

oxyanion strand upon PRFAR binding is likely conferred through the backbone–backbone interaction between A393 and N52 (Figure 2b) and is regulated by the binding of the PRFAR substrate in the cyclase active site.

Mechanism of Glutaminase Stimulation. From the body of the available experimental and computational data, we suggest the following scenario to describe the regulation of the glutaminase activity in IGP synthase. The main dynamic feature of this process is reflected by the kinetic properties of the enzyme which indicate that glutamine binding–commitment to hydrolysis is modulated by a signaling event from the cyclase active site upon binding of PRFAR. The glutamine substrate enters the active site to interact with the nucleophilic elbow at C83 (Figure 5a). When PRFAR binds, there is a general tightening of the interdomain region. Glutamine substrate recognition is achieved through interaction with both Q87 and Q397, which helps to properly orient the binding substrate (Figure 5b). As the two subdomains come together, an additional interaction between the cyclase A393 and glutaminase N52 on the oxyanion strand forms the oxyanion hole at G50. The catalytic triad residues H193 and E195 are pushed toward C83 by the interaction between D359 and K196. Glutamine hydrolysis is initiated when the imidazole ring of H193 is within 3 Å of the thioester (Figure 5b). Ammonia is released and travels through the protein to the waiting PRFAR. Release of the cyclase products creates a relaxation in the protein, opening the interdomain chamber to release the glutamate product (Figure 5c).

Conservation of Structural Features in the Triad Glutamine Amidotransferase Family. In this study of IGP synthase, we have shown that an interdomain contact at the glutaminase loop containing the catalytic histidine and glutamic acid is essential for the stimulation of glutaminase activity when the acceptor substrate is bound. The glutaminase domain is highly conserved in all triad amidotransferases, and in several of these proteins, charged residues from the acceptor domain interact with this same glutaminase loop and are directly linked to the acceptor active site (Table 6). In CTP synthetase, H314 is downstream from the ATP binding site residue D303 (13). The synthetase reaction in CTPS is catalyzed through phosphorylation of O4 on UTP. In anthranilate synthase D275 is downstream from D266, a catalytically essential residue in anthranilate synthesis (45). D266 resides in the chorismate active site in subdomain IIb (12). In FGAR-amidotransferase, D657 is downstream from Mg-ADP binding site residue E348 (12, 14). The binding of ADP is essential for the formation of the active FGAR-amidotransferase complex (46). Due to the mechanistic and structural complexity of the trisubstrate enzyme carbamoyl phosphate synthetase, it is difficult to offer a theory of reaction coupling in this protein. GMP synthetase was also excluded from this analysis since it is expected to undergo major structural changes in the activated form.

The studies described in this paper represent a focused investigation into the coupling of the two reactions in a triad glutamine amidotransferase. We have shown in IGP synthase that an interdomain contact at the glutaminase loop containing the histidine and glutamic acid of the catalytic triad is key to triggering glutamine hydrolysis when the acceptor substrate is bound in the second active site. We have identified in other triad glutamine amidotransferases similar interdomain contacts directly linked to the acceptor active

sites that may also function in coupling the two reactions. Further studies into these structural features in other triad glutamine amidotransferases may show this to be another unifying feature of this fascinating family of proteins.

ACKNOWLEDGMENT

We thank Justin Oliver, Vishal Nashine, and Giselle Knudsen for many helpful discussions of the manuscript.

SUPPORTING INFORMATION AVAILABLE

Experimental details. This material is available free of charge via the Internet at <http://pubs.acs.org>.

REFERENCES

- Klem, T. J., and Davisson, V. J. (1993) Imidazole glycerol phosphate synthase: the glutamine amidotransferase in histidine biosynthesis, *Biochemistry* 32, 5177–86.
- Zalkin, H., and Smith, J. (1998) Enzymes using glutamine as an amide donor, *Adv. Enzymol. Relat. Areas Mol. Biol.* 72, 87–144.
- Chaudhuri, B. N., Lange, S. C., Myers, R. S., Chittur, S. V., Davisson, V. J., and Smith, J. L. (2001) $(\beta/\alpha)_8$ barrel joins two active sites, *Structure* 9, 987–997.
- Douangamath, A., Walker, M., Beismann-Driemeyer, S., Vega-Fernandez, M. C., Sterner, R., and Wilmanns, M. (2002) Structural evidence for ammonia tunneling across the $(\beta/\alpha)_8$ barrel of the imidazole glycerol phosphate synthase bienzyme complex, *Structure* 10, 185–193.
- Omi, R., Mizuguchi, H., Goto, M., Miyahara, I., Hayashi, H., Kagamiyama, H., and Hirotsu, K. (2002) Structure of imidazole glycerol phosphate synthase from *Thermus thermophilus* HB8: open-closed conformational change and ammonia tunneling, *J. Biochem. (Tokyo)* 132, 759–765.
- Amaro, R., Tajkhorshid, E., and Luthey-Schulten, Z. (2003) Developing an energy landscape for the novel function of a $(\beta/\alpha)_8$ barrel: ammonia conduction through HisF, *Proc. Natl. Acad. Sci. U.S.A.* 100, 7599–7605.
- Amaro, R., and Luthey-Schulten, Z. (2004) Molecular dynamics simulations of substrate channeling through an α/β barrel protein, *Chem. Phys.* 307, 147–155.
- Chaudhuri, B. N., Lange, S. C., Myers, R. S., Davisson, V. J., and Smith, J. L. (2003) Toward understanding the mechanism of the complex cyclization reaction catalyzed by imidazole glycerol phosphate synthase: crystal structures of a ternary complex and the free enzyme, *Biochemistry* 42, 7003–7012.
- Morollo, A. A., and Eck, M. J. (2001) Structure of the cooperative allosteric anthranilate synthase from *Salmonella typhimurium*, *Nat. Struct. Biol.* 8, 243–247.
- Tesmer, J. J. G., Klem, T. J., Deras, M. L., Davisson, V. J., and Smith, J. L. (1996) The crystal structure of GMP synthetase reveals a novel catalytic triad and is a structural paradigm for two enzyme families., *Nat. Struct. Biol.* 3, 74–86.
- Thoden, J. B., Holden, H. M., Wesenberg, G., Raushel, F. M., and Rayment, I. (1997) Structure of carbamoyl phosphate synthetase: a journey of 96 Å from substrate to product, *Biochemistry* 36, 6305–6316.
- Knochel, T., Ivens, A., Hester, G., Gonzalez, A., Bauerle, R., Wilmanns, M., Kirschner, K., and Jansonius, J. N. (1999) The crystal structure of anthranilate synthase from *Sulfolobus solfataricus*: functional implications, *Proc. Natl. Acad. Sci. U.S.A.* 96, 9479–9484.
- Endrizzi, J. A., Kim, H., Anderson, P. M., and Baldwin, E. P. (2004) Crystal structure of *Escherichia coli* cytidine triphosphate synthetase, a nucleotide-regulated glutamine amidotransferase/ATP-dependent amidoligase fusion protein and homologue of anticancer and antiparasitic drug targets, *Biochemistry* 43, 6447–6463.
- Anand, R., Hoskins, A. A., Stubbe, J., and Ealick, S. E. (2004) Domain organization of *Salmonella typhimurium* formylglycinamide ribonucleotide amidotransferase revealed by X-ray crystallography, *Biochemistry* 43, 10328–10342.
- Huang, X., Holden, H. M., and Raushel, F. M. (2001) Channeling of substrates and intermediates in enzyme-catalyzed reactions, *Annu. Rev. Biochem.* 70, 149–180.

16. Myers, R. S., Jensen, J. R., Deras, I. L., Smith, J. L., and Davisson, V. J. (2003) Substrate-induced changes in the ammonia channel for imidazole glycerol phosphate synthase, *Biochemistry* 42, 7013–7022.
17. Roux, B., and Walsh, C. T. (1992) *p*-Aminobenzoate synthesis in *Escherichia coli*: kinetic and mechanistic characterization of the amidotransferase PabA, *Biochemistry* 31, 6904–6910.
18. Chaparian, M. G., and Evans, D. R. (1991) The catalytic mechanism of the amidotransferase domain of the syrian hamster multifunctional protein CAD, *J. Biol. Chem.* 266, 3387–3395.
19. Willemoes, M. (2003) Thr-431 and Arg-433 are part of a conserved sequence motif of the glutamine amidotransferase domain of CTP synthases and are involved in GTP activation of the *Lactococcus lactis* enzyme, *J. Biol. Chem.* 278, 9407–9411.
20. Nakamura, J., Straub, K., Wu, J., and Lou, L. (1995) The glutamine hydrolysis function of human GMP synthetase, *J. Biol. Chem.* 270, 23450–23455.
21. Chittur, S. V., Klem, T. J., Shafer, C. M., and Davisson, V. J. (2001) Mechanism for acivicin inactivation of triad glutamine amidotransferases, *Biochemistry* 40, 876–887.
22. Chittur, S. V., Chen, Y., and Davisson, V. J. (2000) Expression and purification of imidazole glycerol phosphate synthase from *Saccharomyces cerevisiae*, *Protein Expression Purif.* 18, 366–377.
23. Hirschbein, B. L., Mazonod, F. P., and Whitesides, G. M. (1982) Synthesis of phosphoenolpyruvate and its use in adenosine triphosphate cofactor regeneration, *J. Org. Chem.* 47, 3765–3766.
24. Kunkel, T. A. (1985) Rapid and efficient site-specific mutagenesis without phenotypic selection, *Proc. Natl. Acad. Sci. U.S.A.* 82, 488–492.
25. Gleitz, J., Tosch, C., and Peters, T. (1996) Continuous enzyme-linked fluorometric detection of L-(+)-lactate released from rat brain vesicles under anoxic conditions, *J. Neurosci. Methods* 67, 97–102.
26. Gray, P. J., and Duggleby, R. G. (1989) Analysis of kinetic data for irreversible enzyme inhibition, *Biochem. J.* 257, 419–424.
27. Humphrey, W., Dalke, A., and Schulten, K. (1996) VMD—visual molecular dynamics, *J. Mol. Graph.* 14, 33–38.
28. MacKerell, A. (2003), <http://www.psc.edu/general/software/packages/charmm/tutorial/index.html>.
29. MacKerell, A. (2003), <http://www.psc.edu/general/software/packages/charmm/tutorial/mackerell/parameters.html>.
30. Kale, L., Skeel, R., Bhandarkar, M., Brunner, R., Gursoy, A., Krawetz, N., Phillips, J., Shinozaki, A., Varadarajan, K., and Schulten, K. (1999) NAMD2: Greater Scalability for Parallel Molecular Dynamics, *J. Comput. Phys.* 151, 283–312.
31. Grubmuller, H. (1996), Theoretical Biophysics Group, Institute for Medical Optics, Ludwig-Maximilians University, Munich.
32. MacKerell, A. D., Jr., Bashford, D., Bellott, M., Dunbrack, R. L., Jr., Evanseck, J. D., Field, M. J., Fischer, S., Gao, J., Guo, H., Ha, S., Joseph-McCarthy, D., Kuchnir, L., Kuczera, K., Lau, F. T. K., Mattos, C., Michnick, S., Ngo, T., Nguyen, D. T., Prodhom, B., Reiher, W. E., III, Roux, B., Schlenkrich, M., Smith, J. C., Stote, R., Straub, J., Watanabe, M., Wiorkiewicz-Kuczera, J., Yin, D., and Karplus, M. (1998) All-Atom Empirical Potential for Molecular Modeling and Dynamics Studies of Proteins, *J. Phys. Chem. B* 102, 3586–3616.
33. Darden, T., York, D., and Pedersen, L. (1993) *J. Chem. Phys.* 98, 10089–10092.
34. Lang, D., Thoma, R., Henn-Sax, M., Sterner, R., and Wilmanns, M. (2000) Structural evidence for evolution of the β/α barrel scaffold by gene duplication and fusion, *Science* 289, 1546–1550.
35. Huang, X., and Raushel, F. M. (1999) Deconstruction of the catalytic array within the amidotransferase subunit of carbamoyl phosphate synthetase, *Biochemistry* 38, 15909–15914.
36. Klem, T. J., Chen, Y., and Davisson, V. J. (2001) Subunit interactions and glutamine utilization by *Escherichia coli* imidazole glycerol phosphate synthase, *J. Bacteriol.* 183, 989–996.
37. Amaro, R., Myers, R. S., Davisson, V. J., and Luthey-Schulten, Z. (2005) Evidence of the allosteric effect in IGP synthase, manuscript in preparation.
38. Amaro, R. E., Myers, R. S., Davisson, V. J., and Luthey-Schulten, Z. A. (2005) Structural elements in IGP synthase exclude water to optimize ammonia transfer, *Biophys. J.* 89, 475–487.
39. Korolev, S., Skarina, T., Evdokimova, E., Edwards, A., Joachimiak, A., and Savchenko, A. (2002) Crystal structure of glutamine amidotransferase from *Thermotoga maritima*, *Proteins: Struct., Funct., Genet.* 49, 420–422.
40. Saeed-Kothe, A., and Powers-Lee, S. G. (2002) Specificity determining residues in ammonia- and glutamine-dependent carbamoyl phosphate synthetases, *J. Biol. Chem.* 277, 7231–7238.
41. Saeed-Kothe, A., and Powers-Lee, S. G. (2003) Gain of glutaminase function in mutants of the ammonia-specific frog carbamoyl phosphate synthetase, *J. Biol. Chem.* 278, 26722–26726.
42. Mathews, D. A., Alden, R. A., Birktoft, J. J., Freer, S. T., and Kraut, J. (1975) X-ray crystallographic study of boronic acid adducts with subtilisin BPN' (Novo): a model for the catalytic transition state, *J. Biol. Chem.* 250, 7120–7126.
43. Thoden, J. B., Miran, S. G., Phillips, J. C., Howard, A. J., Raushel, F. M., Holden, H. M. (1998) Carbamoyl phosphate synthetase: caught in the act of glutamine hydrolysis, *Biochemistry* 37, 8825–8831.
44. Barrette-Ng, I. H., Ng, K. K.-S., Mark, B. L., van Aken, D., Cherney, M. M., Garen, C., Kolodenko, Y., Gorbalenya, A. E., Snijder, E. J., and James, M. N. G. (2002) Structure of Arterivirus nsp4: the smallest chymotrypsin-like proteinase with an α/β C-terminal extension and alternate conformations of the oxyanion hole, *J. Biol. Chem.* 277, 39960–39966.
45. Morollo, A. A., and Bauerle, R. (1993) Characterization of composite aminodeoxyisochorismate synthase and aminodeoxyisochorismate lyase activities of anthranilate synthase, *Proc. Natl. Acad. Sci. U.S.A.* 90, 9983–9987.
46. Hoskins, A. A., Anand, R., Ealick, S. E., and Stubbe, J. (2004) The formylglycinamide ribonucleotide amidotransferase complex from *Bacillus subtilis*: metabolite-mediated complex formation, *Biochemistry* 43, 10314–10327.

BI050706B